CYBERNETICS AND PHYSICS, VOL. 14, NO. 4, 2025, 407–413

CONTROL OF A TWO-ROTOR VIBRATION SYSTEM WITH NON-IDENTICAL ROTORS AND AN ELASTICALLY ATTACHED MASS

Dmitry Tomchin
Institute for Problems in Mechanical Engineering
of the Russian Academy of Sciences,
St. Petersburg, Russian Federation
tda@ipme.ru

Dmitry Gorlatov
Saint Petersburg State University of Architecture
and Civil Engineering (SPSUACE),
St. Petersburg, Russian Federation

Article history:
Received 05.12.2025, Accepted 20.12.2025

Abstract

The study investigates a model of the dynamics of a two-rotor vibrating system (VS) with rotors of different masses and a non-stationary elastically attached mass. It is assumed that the supporting platform of the VS moves in the vertical plane, taking into account the rotation angle. Using computer modeling, the influence of rotor non-identicality on the stability of the frequency-coordinate synchronization regime is analyzed under various loading conditions. A special synchronization control algorithm, synthesized using the speed-gradient method, is employed in the work to ensure a stable synchronous regime.

Key words

multi-rotor vibration system, non-stationary load, non-identical vibrators, frequency-coordinate synchronization

1 Introduction

One of the problems that arises in the operation of multi-rotor vibration systems (MRVS) is the synchronization of the angular positions of the unbalanced rotors of the vibration exciters [Blekhman, 1994; Blekhman and Fradkov, 2001]. As is known, the synchronization process is influenced by many factors: the manufacturing accuracy of the unbalanced rotors, the method of loading the vibration system, and so on. A stable synchronous rotation of the vibration exciter rotors allows for the maximum amplitude of the sieves' oscillations with bulk material being sifted at the same energy expenditure [Blekhman, 1994].

Additional possibilities for various technological processes are provided by system asymmetry. In particular, for processes such as vibrational transport of dusty, wet, and sticky materials, where it is desirable to ensure complex trajectories of the working element. Asymmetry can be introduced either programmatically or physically by using non-identical unbalanced vibration exciters (UVEs). Maintaining a stable synchronous mode can be achieved using special control algorithms. In the development of such control algorithms, the speed gradient method has proven to be effective [Blekhman and Fradkov, 2001; Andrievsky et al., 1996; Miroshnik et al., 2000; Andrievsky and Fradkov, 2021; Borisenok and Gogoleva,]. Some interesting results can be found in [Tomchina, 2023; Zaitceva et al., 2023].

In this work, the dynamics of a two-rotor vibration system with non-identical rotors and a non-stationary mass are considered. Taking into account the dynamics of the mass in the vibration system model allows for a more effective evaluation of the quality of the control algorithms. To study these processes, the SV-2 vibration test bench was created. The mass of the sifted material was considered in its design as an additional non-stationary load, attached via an elastic connection. The other related approaches to the problem can be found in [Zaitceva et al., 2025; Shagniev, 2025].

2 Synthesis of the dynamic model of a multi-rotor vibration system (MRVS)

In this section, based on the design of the mechanical part of the SV-2/SV-2M vibration test bench, models of the multi-rotor vibration system (MRVS) are derived. Figure 1 shows the vibration test bench under study, with a detailed description provided in [Blekhman, 1994; Blekhman and Fradkov, 2001]. Unlike the original two-rotor SV-2/SV-2M scheme, the computational MRVS scheme, shown in Figure 2, allows for an increase in the number of rotors up to n.

The coordinate system associated with the platform is denoted as $0'x'y'$. The coordinates of the platform center (point 0') are $\{x_c, y_c\}$. The platform is mounted on

elastic supports (springs). The abscissas of the spring attachments are $x_{ni} = \pm a$. The axes of rotor rotation are perpendicular to the plane of motion and are assumed to be strictly horizontal. Therefore, the displacement of the MRVS along the $0z$ axis is not considered in this model. Consequently, the four elastic supports can be represented as two springs with corresponding equivalent stiffness c_{0i}, neglecting their transverse stiffness along the $0z$ axis and torsion.

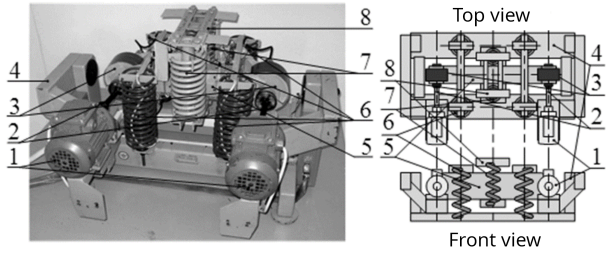

Figure 1. Mechanical part of the SV-2/SV-2M vibration test bench: 1 — electric motors driving the rotors; 2 — cardan shafts connecting motors and rotors; 3 — unbalanced rotors; 4 — supporting frame; 5 — platform (vibrating working body); 6 — lower springs isolating the platform from the frame; 7 — upper springs for load attachment; 8 — load support base.

In Figure 2, the following notations are used: x_c, y_c, φ, φ_i, $i = 1, \ldots, n$ are the generalized coordinates of the system, where $x_{c0} = 0$, $y_{c0} = 0$ are the coordinates of the center of mass of the supporting body (platform) of the MVM in a Cartesian coordinate system rigidly attached to the foundation; φ is the rotation angle of the platform in the vertical plane $0xy$, measured counterclockwise; φ_i is the rotation angle of the i-th unbalance about the motor axis, measured counterclockwise; M_i is the driving torque of the i-th motor; $k_c\dot{\varphi}_i$ is the resisting torque of the i-th unbalance; m_s is the mass of the MVM platform; m_i is the mass of the i-th unbalance; ϱ_i is the eccentricity of the i-th unbalance relative to the rotation axis; r_i is the distance from the platform center of mass to the rotation axis of the i-th unbalance; c_{01}, c_{02} are the equivalent stiffness coefficients of the elastic supports along the vertical and horizontal axes; β is the damping coefficient in the springs; k_c is the viscous friction coefficient in the bearings of the vibration exciters; g is the gravitational acceleration; ΔU_1, ΔU_2 are the spring elongations.

The rotors in this model may have identical or different mass–inertial parameters (m_i and ϱ_i, $i = 1, \ldots, n$). m_L is the mass of the load; x_L, y_L are the coordinates of the load center of mass; c_{11} and c_{12} are the horizontal and vertical stiffness coefficients of the upper spring connecting the load to the platform.

The coordinates of the centers of mass of the unbalanced rotors in the fixed coordinate system are expressed as:

$$\begin{aligned} x_i &= x_c + r_i \cos\varphi + \varrho_i \cos(\varphi + \varphi_i), \\ y_i &= y_c + r_i \sin\varphi + \varrho_i \sin(\varphi + \varphi_i). \end{aligned} \tag{1}$$

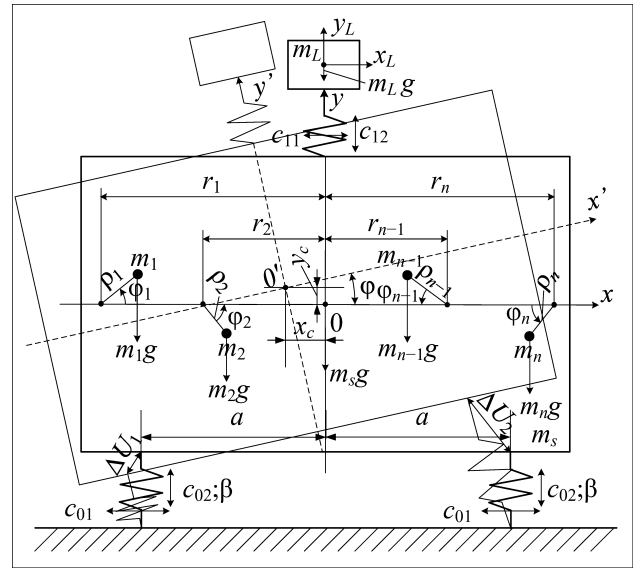

Figure 2. Computational model of the MVM with load (front view).

The kinetic energy of the system is given by:

$$\begin{aligned} T = {} & \tfrac{1}{2} m_0 \dot{x}_c^2 + \tfrac{1}{2} m_0 \dot{y}_c^2 + 0.5 \dot{x}_L^2 m_0 + \tfrac{1}{2} \dot{y}_L^2 m_0 + \\ & \tfrac{1}{2} J \dot{\varphi}^2 + \dot{\varphi}^2 \sum_{i=1}^{n} m_i r_i \varrho_i \cos\varphi_i + 0.5 \sum_{i=1}^{n} J_i \dot{\varphi}_i^2 + \\ & \dot{\varphi} \sum_{i=1}^{n} J_i \dot{\varphi}_i + \sum_{i=1}^{n} [\dot{\varphi}\dot{\varphi}_i m_i r_i \varrho_i \cos\varphi_i - \\ & \dot{x}_c \dot{\varphi} m_i r_i \sin\varphi_i + \dot{x}_c \dot{\varphi} m_i \varrho_i \sin(\varphi + \varphi_i) - \\ & \dot{x}_c \dot{\varphi}_i m_i \varrho_i \sin(\varphi + \varphi_i) + \dot{y}_c \dot{\varphi}_i m_i r_i \cos\varphi + \\ & \dot{y}_c \dot{\varphi} m_i \varrho_i \cos(\varphi + \varphi_i) + \dot{y}_c \dot{\varphi}_i m_i \varrho_i \cos(\varphi + \varphi_i)]. \end{aligned} \tag{2}$$

where $m_0 = m_s + \sum_{i=1}^{n}(m_i)$, $J_i = J_{ci} + m_i \varrho_i^2$ and $J = J_s + \sum_{i=1}^{n} J_i + \sum_{i=1}^{n} \left(m_i r_i^2\right)$ are the moments of inertia of the i-th rotor and the platform, respectively.

The potential energy of the MVM has the form:

$$\begin{aligned} \Pi = {} & m_0 g y_c + m_L g y_L + g \sum_{i=1}^{n} (m_i r_i \sin\varphi + \\ & m_i \varrho_i \sin(\varphi + \varphi_i)) + c_{01} \left(x_c^2 + a^2 \cos^2\varphi\right) + c_{02} \left(y_c^2 \right. \\ & \left. + a^2 \sin^2\varphi\right) + \tfrac{1}{2} c_{11} (x_c - x_L)^2 + \tfrac{1}{2} c_{12} (y_c - y_L)^2. \end{aligned} \tag{3}$$

The equations of motion of the MVM, obtained in the form of Lagrange equations of the second kind, are writ-

ten as:

$$
\begin{aligned}
&m_0\ddot{x}_c + \sum_{i=1}^{n} (\dot{\varphi} m_i r_i \sin\varphi - \dot{\varphi} m_i \varrho_i \sin(\varphi+\varphi_i) - \\
&\dot{\varphi}_i m_i \varrho_i \sin(\varphi+\varphi_i) - \dot{\varphi}^2 m_i r_i \cos\varphi - \\
&\dot{\varphi}^2 m_i \varrho_i \cos(\varphi+\varphi_i) - \dot{\varphi}_i^2 m_i \varrho_i \cos(\varphi+\varphi_i) - \\
&2\dot{\varphi}\dot{\varphi}_i m_i \varrho_i \cos(\varphi+\varphi_i)) + 2c_{01}x_c + c_{11}(x_c - x_L) + \\
&\beta\dot{x}_c = 0; \\
&m_0\ddot{y}_c + \sum_{i=1}^{n} (\dot{\varphi} m_i r_i \cos\varphi + \dot{\varphi} m_i \varrho_i \cos(\varphi+\varphi_i) + \\
&\dot{\varphi}_i m_i \varrho_i \cos(\varphi+\varphi_i) - \dot{\varphi}^2 m_i r_i \sin\varphi - \\
&\dot{\varphi}^2 m_i \varrho_i \sin(\varphi+\varphi_i) - \dot{\varphi}_i^2 m_i \varrho_i \sin(\varphi+\varphi_i) - \\
&2\dot{\varphi}\dot{\varphi}_i m_i \varrho_i \sin(\varphi+\varphi_i)) + m_0 g + 2c_{02}y_c + \\
&c_{12}(y_c - y_L) + \beta\dot{y}_c = 0; \\
&J\ddot{\varphi} + 2\dot{\varphi}\sum_{i=1}^{n} m_i r_i \varrho_i \cos\varphi_i + \sum_{i=1}^{n} J_i\ddot{\varphi}_i + \\
&\sum_{i=1}^{n} [\ddot{\varphi}_i m_i r_i \varrho_i \cos\varphi_i - \ddot{x}_c m_i r_i \sin\varphi - \\
&\ddot{x}_c m_i \varrho_i \sin(\varphi+\varphi_i) + \ddot{y}_c m_i r_i \cos\varphi + \\
&\ddot{y}_c m_i \varrho_i \cos(\varphi+\varphi_i) - \dot{\varphi}_i^2 m_i r_i \varrho_i \sin\varphi_i] + \\
&2\dot{\varphi}\sum_{i=1}^{n} (-\dot{\varphi}_i m_i r_i \varrho_i \sin\varphi_i) + \\
&g\sum_{i=1}^{n} [m_i r_i \cos\varphi + m_i \varrho_i \cos(\varphi+\varphi_i)] - \\
&a^2(c_{01} - c_{02})\sin 2\varphi + \beta\dot{\varphi} = 0; \\
&-\ddot{x}_c m_i \varrho_i \sin(\varphi+\varphi_i) + \ddot{y}_c m_i \varrho_i \cos(\varphi+\varphi_i) + \\
&\ddot{\varphi}\,(J_i + m_i r_i \varrho_i \cos\varphi_i) + J_i\ddot{\varphi}_i + \dot{\varphi}^2 m_i r_i \varrho_i \sin\varphi_i + \\
&m_i g \varrho_i \cos(\varphi+\varphi_i) + k_c\dot{\varphi}_i = M_i; \\
&m_L\ddot{x}_L - c_{11}\,(x_c - x_L) + \dot{m}_l\dot{x}_L + \beta\dot{x}_L = F_x; \\
&m_L\ddot{y}_L + \dot{m}_l\dot{y}_L + m_L g - c_{12}\,(y_c - y_L) + +\beta\dot{y}_L = F_y,
\end{aligned}
\tag{4}
$$

where M_i are the control moments, $i = 1, \ldots, n$; F_x and F_y are the projections onto the $0x$ and $0y$ axes of the resultant external force F, caused by the velocity and mass of the processed material falling from the platform.

3 Synthesis of synchronization algorithms for a two-rotor vibratory system with a nonstationary load

Integral-differential speed gradient algorithms, particular cases of which are proportional, integral, and proportional-integral speed gradient algorithms, are described in [Fradkov et al., 2013].

In this work, a proportional-integral speed gradient algorithm is applied for synchronization, synthesized for the vibratory system model taking into account a nonstationary load.

Important types of synchronization for vibratory systems are frequency and coordinate synchronization of vibratory exciters.

Frequency synchronization is understood as the exact matching of the exciter speeds:

$$\omega_s = \omega_r; \qquad s, r = 1, \ldots, k. \tag{5}$$

In practice, approximate synchronization is considered:

$$|\omega_s - \omega_r| \le \varepsilon, \tag{6}$$

where $\varepsilon > 0$ can be chosen as $\varepsilon = 0.05\,\omega^*$, analogously to the given accuracy in the conventional definition of the transient process time.

Coordinate synchronization occurs when the outputs or certain phase coordinates of one of the vibratory exciter subsystems coincide, up to constant values, with the corresponding coordinates of other subsystems for all $t \ge t_0$; that is, the exciter phases φ_i, $i = 1, \ldots, k$, satisfy the identities:

$$\varphi_s(t) - \varphi_r(t) = L_{sr}, \quad s, r = 1, \ldots, k. \tag{7}$$

In practical problems, expression (7) is replaced with an approximate one:

$$|\varphi_s(t) - \varphi_r(t) - L_{sr}| < \varepsilon_1, \quad s, r = 1, \ldots, k. \tag{8}$$

The system is said to exhibit *approximate frequency-coordinate synchronization* if conditions (6) and (8) hold simultaneously for some $\varepsilon > 0$, $\varepsilon_1 > 0$, and $L_{sr} = \text{const}$ [Fradkov et al., 2013].

This work is devoted to solving the problem of synthesizing a controlled algorithm for approximate frequency-coordinate synchronization of a nonstationary vibratory system with non-identical rotors.

According to the speed gradient scheme [Fradkov et al., 2013], we obtain the equation for calculating control torques:

$$
\begin{cases}
M_1 = -\gamma_1 \left[(1-\alpha)\,(H - H^*)\,\dot{\varphi}_1 + \right. \\
\quad \left. \frac{\alpha}{J_1}\,(\dot{\varphi}_1 \pm \dot{\varphi}_2) + \frac{\alpha}{J_1}\,(\varphi_1 \pm \varphi_2 + \Delta\varphi_{*1})\right] \\
M_2 = -\gamma_2 \left[(1-\alpha)\,(H - H^*)\,\dot{\varphi}_2 + \right. \\
\quad \left. \frac{\alpha}{J_2}\,(\dot{\varphi}_1 \pm \dot{\varphi}_2) + \frac{\alpha}{J_2}\,(\varphi_1 \pm \varphi_2 + \Delta\varphi_{*2})\right],
\end{cases}
\tag{9}
$$

where φ_* is the integration constant, H^* is the given total mechanical energy of the system.

Since the expression for the total mechanical energy H is cumbersome, it is reasonable to reduce it for simplifying the calculation of control actions. It is assumed that this simplification weakly affects the closed-loop system dynamics due to the robust properties of speed gradient algorithms.

Finally, the electromechanical control torques are calculated as:

$$
\begin{cases}
M_1 = -\gamma_1 \left[(1-\alpha)\,\left(\overline{H} - H^*\right)\,\dot{\varphi}_1 + \right. \\
\quad \left. \frac{\alpha}{J_1}\,(\dot{\varphi}_1 \pm \dot{\varphi}_2) + \frac{\alpha}{J_1}\,(\varphi_1 \pm \varphi_2 + \Delta\varphi_{*1})\right] \\
M_2 = -\gamma_2 \left[(1-\alpha)\,\left(\overline{H} - H^*\right)\,\dot{\varphi}_2 + \right. \\
\quad \left. \frac{\alpha}{J_2}\,(\dot{\varphi}_1 \pm \dot{\varphi}_2) + \frac{\alpha}{J_2}\,(\varphi_1 \pm \varphi_2 + \Delta\varphi_{*2})\right],
\end{cases}
\tag{10}
$$

where $\overline{H}$ is the reduced mechanical energy of the vibratory system with non-identical rotors:

$$
\begin{aligned}
&\overline{H} = \tfrac{1}{2}m_0\dot{x}_c^2 + \tfrac{1}{2}m_0\dot{y}_c^2 + \tfrac{1}{2}J_1\dot{\varphi}_1^2 + \tfrac{1}{2}J_2\dot{\varphi}_2^2 - \\
&m_1\varrho_1 \sin\varphi_1\dot{x}_c\dot{\varphi}_1 + m_2\varrho_2\cos\varphi_2\dot{y}_c\dot{\varphi}_2 - \\
&m_2\varrho_2\sin\varphi_2\dot{x}_c\dot{\varphi}_2 + m_1\varrho_1\cos\varphi_1\dot{y}_c\dot{\varphi}_1 + \\
&m_0 g y_c + m_1\varrho_1 g\sin\varphi_1 + m_2\varrho_2 g\sin\varphi_2 + \\
&c_{01}\left(x_c^2 + \alpha^2\right) + c_{02}y_c^2.
\end{aligned}
\tag{11}
$$

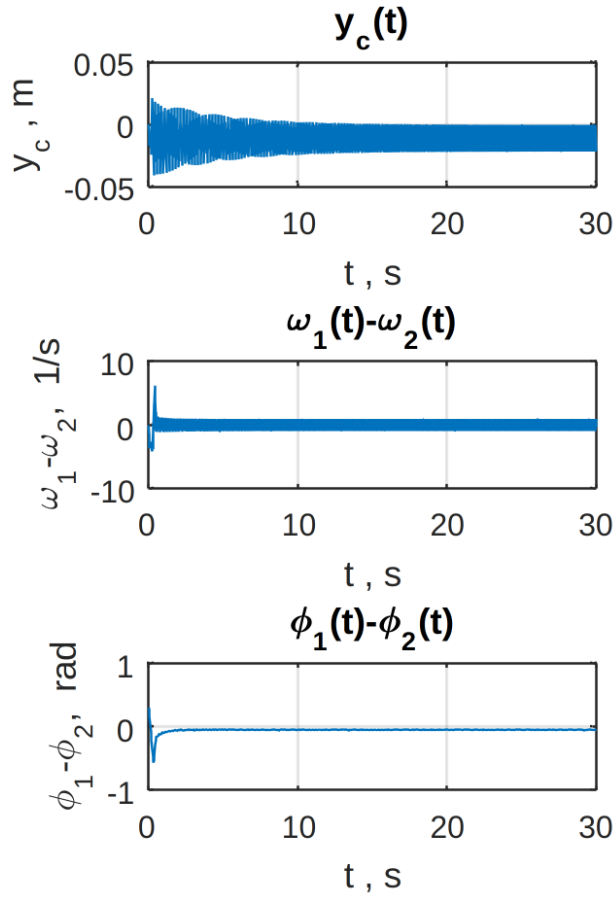

Figure 3. Simulation results without load for $m_1 = m_2 = 1.5$ kg.

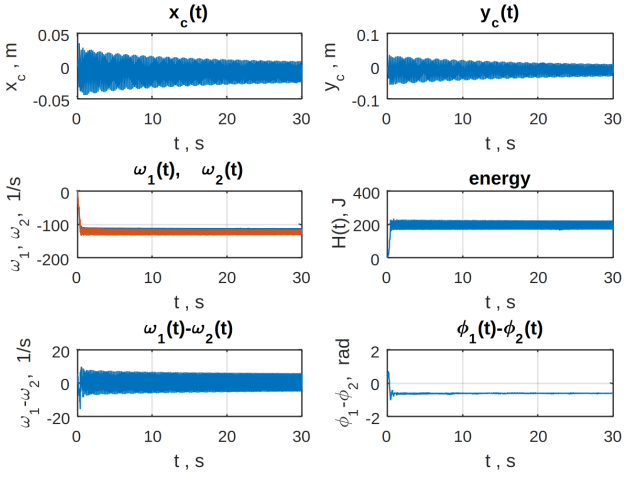

Figure 4. Simulation results without load for $m_1 = 1.5$ kg, $m_2 = 2.5$ kg.

4 Results of computer simulation of the dynamics of a two-rotor vibratory system with non-identical rotors and variable load

This section presents the results of studying the dynamics of a vibratory system with rotors differing in mass and a variable load, obtained from the analysis of system (4) in MATLAB.

It is assumed that loading does not start at the moment of system start-up but after the system reaches the operating regime at time t_1, which exceeds the time of initial rotor synchronization. The mass of the bulk material (load) changes starting from time t_1. Before this moment, the load mass is constant (corresponding to the mass of the loaded tray).

The load is considered as an elastically attached point mass. During the simulation, the stability of the synchronous mode was analyzed depending on the average loading rate and the established average load mass. It is assumed that at time t_2 the average amount of material being added approximately equals the amount removed from the platform, leading to a practically constant load mass for $t > t_2$.

The reduced expression for the mechanical energy (11) allows calculating the control torques based on the positions and velocities of the platform and rotors. Platform velocity information can be obtained using an observer similar to that described in [Fradkov et al., 2016]. Thus, the synchronization algorithm (10) can be practically implemented.

The system parameters corresponded to the SV-2 test stand: $m_s = 9$ kg, $g = 9.81$ m/s^2, $c_{01} = c_{02} = 5300$ N/m, $c_{11} = c_{12} = 2650$ N/m, $k_c = 0.01$ J/s, $\beta = 5$ kg/s, $J_1 = J_2 = 0.014$ kg·m^2, $m_L(0) = 1$ kg, $m_1 = m_2 = 1.5$ kg, $\varrho_1 = \varrho_2 = 0.04$ m.

The existence of a stable synchronous mode was confirmed by plots of the difference in angular velocities $(\dot\varphi_1 - \dot\varphi_2)$ and the phase difference $\Delta\varphi = \varphi_1 - \varphi_2$. As seen from the figures, the required relationship between the average speeds is satisfied ($|\omega_s - \omega_r| \le \varepsilon$, where $\omega_i = \dot\varphi_i$), and the phase shift $\Delta\varphi(\infty)$ stabilizes at a constant level, which corresponds to the definition of coordinate synchronization. In the table, the coordinate synchronization time t_{syn} is determined from the phase difference plots as the time at which $\Delta\varphi$ enters the 5% neighborhood of its steady-state value $\Delta\varphi(\infty)$, while the transient time t_{tr} is determined from the rotor angular velocity plots.

At the first stage, the permissible difference in unbalance masses was investigated, at which the synchronization algorithm (10) ensures stable frequency-coordinate synchronization for the system without a load. Algorithm parameters: $\gamma_1 = \gamma_2 = 0.012$, $\alpha_1 = \alpha_2 = 0.25$, $H^* = 200$ J.

The simulation results are shown in Figs. 3–5 and in Table 1. The figures present plots of the horizontal and vertical coordinates of the platform, x_c and y_c; plots of the rotor angular velocities ω_i; plots of the phase and velocity differences of the rotors, $\Delta\varphi = \varphi_1 - \varphi_2$, $(\omega_1 - \omega_2)$; the system energy $H(t)$; and the load mass m_L.

As seen from Table 1, the control algorithm (10) ensures a stable synchronous mode for unbalance masses differing by no more than a factor of two $(m_1 =$

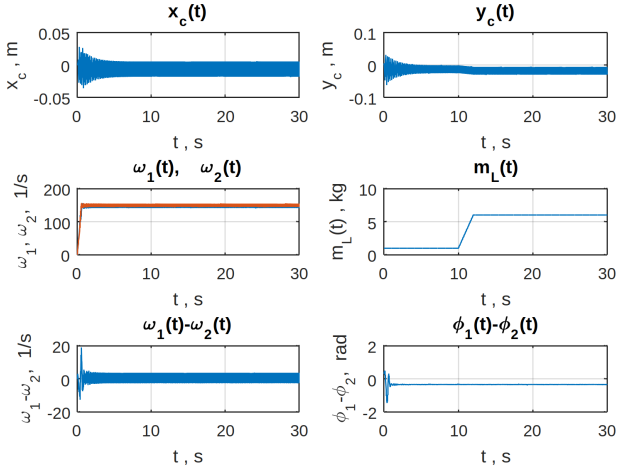

Figure 6. Simulation results of the system with load for $m_1 = 1.5$ kg, $m_2 = 2.5$ kg, $H^* = 300$ J, $V = 2.5$ kg/s, $t_1 = 10$ s, $t_2 = 12$ s.

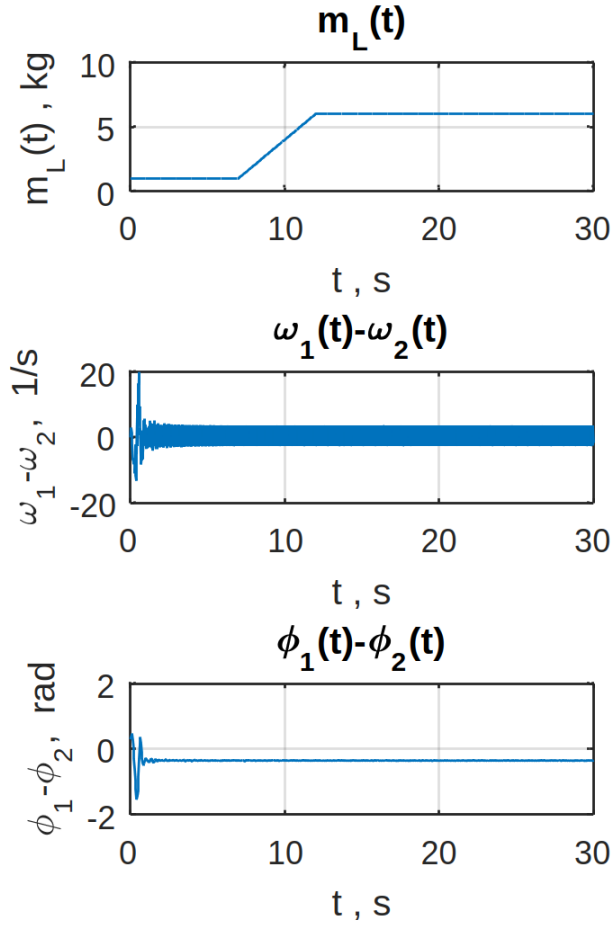

Figure 7. Simulation results of the system with load for $m_1 = 1.5$ kg, $m_2 = 2.5$ kg, $H^* = 300$ J, $V = 1.0$ kg/s, $t_1 = 7$ s, $t_2 = 12$ s.

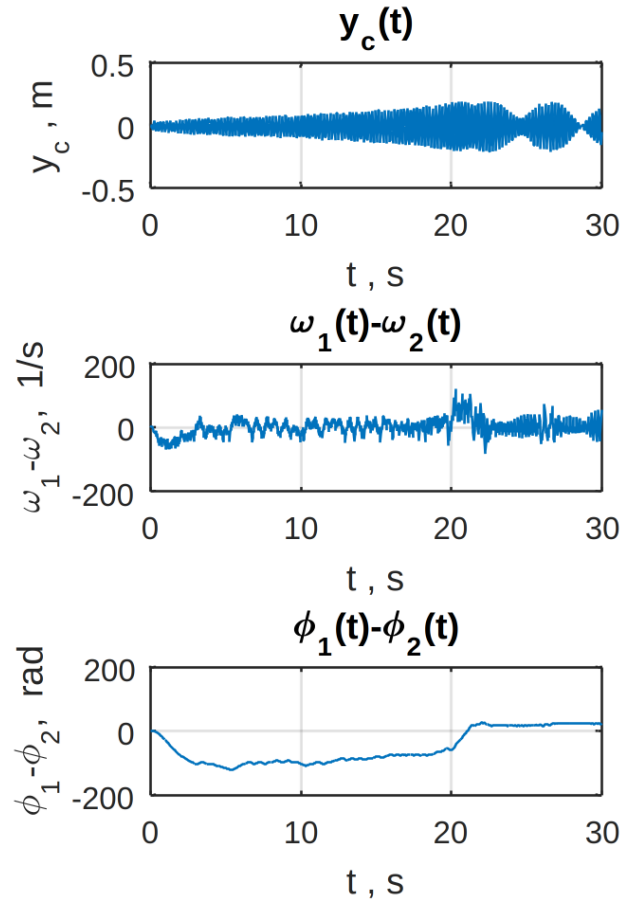

Figure 5. Simulation results without load for $m_1 = 1.0$ kg, $m_2 = 2.5$ kg.

Table 1. Simulation results of the system without load

m_1, m_2 (kg)	t_{syn} (s)	t_{tr} (s)	Range of $y_c(\infty)$ (m)
1.5, 2.5	1.2	0.8	$-0.025 < y_c < 0.005$
1.5, 1.5	0.6	0.5	$-0.020 < y_c < 0$
1.25, 2.5	1.8	1.1	$-0.030 < y_c < 0.010$
1.0, 2.5	—	—	—

$1.25, m_2 = 2.5$). In the case of $m_1 = 1.0$ kg and $m_2 = 2.5$ kg, the synchronous mode is not achieved (Fig. 5). With an increase in the difference between the rotor masses, the values of t_{syn}, t_{tr}, and the oscillation amplitude $y_c(t)$ increase.

At the second stage, the dynamics of the two-rotor vibratory system with non-identical rotors and variable load were studied. The programmed change of mass m_L was defined by the loading rate V. The maximum mass of the attached load, according to the technological specifications of the SV-2 stand, does not exceed 6 kg.

The simulation results are shown in Table 2 and in Figs. 6–8. The tray mass at the initial moment was $m_L(0) = 1$ kg. The average loading rates V ranged from 1 to 2.5 kg/s.

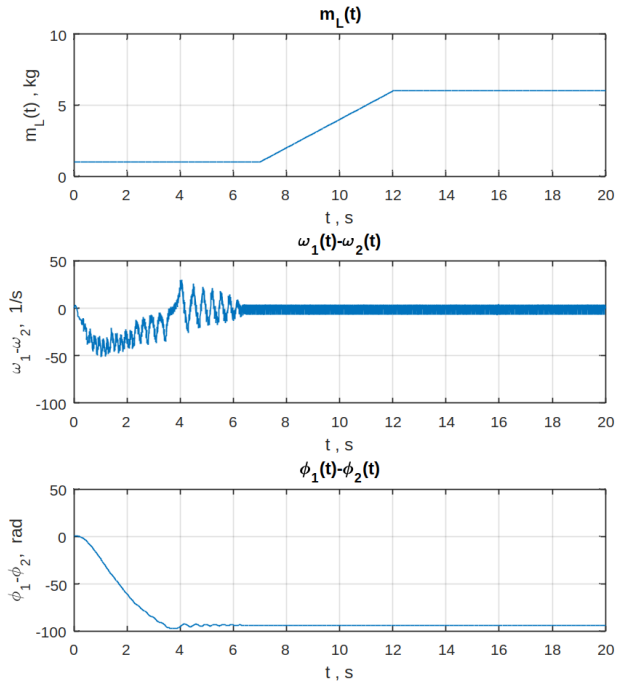

Figure 8. Simulation results of the system with load for $m_1 = 1.5$ kg, $m_2 = 2.5$ kg, $H^* = 300$ J, $V = 1.0$ kg/s, $t_1 = 7$ s, $t_2 = 12$ s.

Table 2. Simulation results of the system with load

m_1, m_2 (kg)	t_1, t_2 (s)	V (kg/s)	t_{syn} (s)	t_{tr} (s)
1.5,2.5	7,12	1.0	1,5	1.2
1.5,2.5	10,12	2.5	1.5	1.2
1.25,2.5	7,12	1.0	4.2	6.25

Thus, if the loading of the tray begins at $t_1 > t_{\text{syn}}$, the variation of $m_L(t)$ does not disturb the established operating regime of the vibrator unit. The transient time for the model with the attached load ($m_L(0) = 1$ kg) is somewhat longer than for the model without the load (Table 1). Since the loading begins after rotor synchronization is achieved, the loading rate does not affect t_{syn} and t_{tr}. At the maximum admissible difference between the rotor masses ($m_1 = 1.25$ kg, $m_2 = 2.5$ kg), the transient time increases sharply in the presence of the load.

5 Conclusion

The presented results of computer simulations allow us to conclude that the synchronization algorithm (10), which uses the reduced expression for energy $\overline{H}$ and does not account for the dynamics of the elastically attached load, ensures a stable synchronous mode. Thus, the proposed approach to implementing control via adaptive speed gradient algorithms, based on simplifying the expression for the total mechanical energy, eliminates the need for sensors measuring load parameters and ensures the achievement of the control objective, as well as the maintenance of a stable synchronous mode under nonstationary loading conditions.

As seen from the presented results, the control algorithm (10) provides a stable synchronous mode for a two-rotor vibratory system with non-identical rotors when the unbalance masses differ by no more than a factor of two. For larger differences, synchronization is not maintained.

Acknoledgements

The research was supported by the Ministry of Science and Higher Education of the Russian Federation (project no. 124041500008-1).

References

Andrievsky, B. R. and Fradkov, A. L. (2021). Speed gradient method and its applications. *Automation and Remote Control*, **82** (9), pp. 1463–1518.

Andrievsky, B. R., Guzenko, P. Y., and Fradkov, A. L. (1996). Control of nonlinear oscillations of mechanical systems by the speed–gradient method (in russian). *Automation and Remote Control*, (4), pp. 4–17.

Blekhman, I. I. (1994). *Vibrational Mechanics (in Russian)*. Nauka, Moscow.

Blekhman, I. I. and Fradkov, A. L., editors (2001). *Control of Mechatronic Vibrational Systems (in Russian)*. Nauka, Saint Petersburg.

Borisenok, S. and Gogoleva, E. Speed gradient control over qubit states. *Cybernetics and Physics*, **13** (3), pp. 193–196.

Fradkov, A. L., Tomchina, O. P., Galitskaya, V. A., and Gorlatov, D. V. (2013). Integral–differentiating speed–gradient algorithms in the problems of multiple synchronization of vibrational systems (in russian). *Scientific and Technical Journal of ITMO*, (1(83)), pp. 30–37.

Fradkov, A. L., Tomchina, O. P., Tomchin, D. A., and Gorlatov, D. V. (2016). Time-varying observer of the supporting body velocity for vibration units. In *6th IFAC Workshop on Periodic Control Systems (PSYCO)*, vol. 49, Austria, IFAC-PapersOnLine, pp. 18–23.

Miroshnik, I. V., Nikiforov, V. O., and Fradkov, A. L. (2000). *Nonlinear and Adaptive Control in Complex Dynamic Systems (in Russian)*. Nauka, Saint Petersburg.

Shagniev, O. (2025). Vibration mechatronic setup with technologic equipment: modeling and reduced energy control. *Cybernetics and Physics*, **14** (4).

Tomchina, O. (2023). Digital control of the synchronous modes of the two-rotor vibration set-up. *Cybernetics and Physics*, **12** (4), pp. 282–288.

Zaitceva, I., Andrievsky, B., and Sivachenko, L. (2023). Enhancing functionality of two-rotor vibration machine by automatic control. *Cybernetics and Physics*, **12** (4), pp. 289–295.

Zaitceva, I., Bushuev, D. A., and Andrievsky, B. (2025). Virtual testing of vibration mechatronic setup with technological accessories. *Cybernetics and Physics*, **14** (4).